Mononuclear Silver Complexes for Efficient Solution and Vacuum-processed OLEDs

Alexander S. Romanov,*[a] Saul T. E. Jones,[b] Le Yang,[b] Patrick J. Conaghan,[b] Dawei Di,[b] Mikko Linnolahti,*[c] Dan Credgington,*[b] and Manfred Bochmann*[a]

[a] Dr. A. S. Romanov https://orcid.org/0000-0003-2617-6402, Prof. Dr. M. Bochmann https://orcid.org/0000-0001-7736-5428, School of Chemistry, University of East Anglia, Earlham Road, Norwich, NR4 7TJ, UK;

[b] P. J. Conaghan 0000-0001-9199-5805, Dr. D. Di https://orcid.org/0000-0003-0703-2809, Dr. L. Yang, S. T. E. Jones https://orcid.org/0000-0001-6007-2530, Dr. D. Credgington https://orcid.org/0000-0003-4246-2118, Department of Physics, Cavendish Laboratory, Cambridge University, Cambridge CB3 0HF, UK

[c] Prof. Dr. M. Linnolahti https://orcid.org/0000-0003-0056-2698, Department of Chemistry, University of Eastern Finland, Joensuu Campus, FI-80101 Joensuu, Finland

Keywords: OLED, silver complex, carbene ligand; photoluminescence; electroluminescence; electrochemistry.

Graphical Abstract:

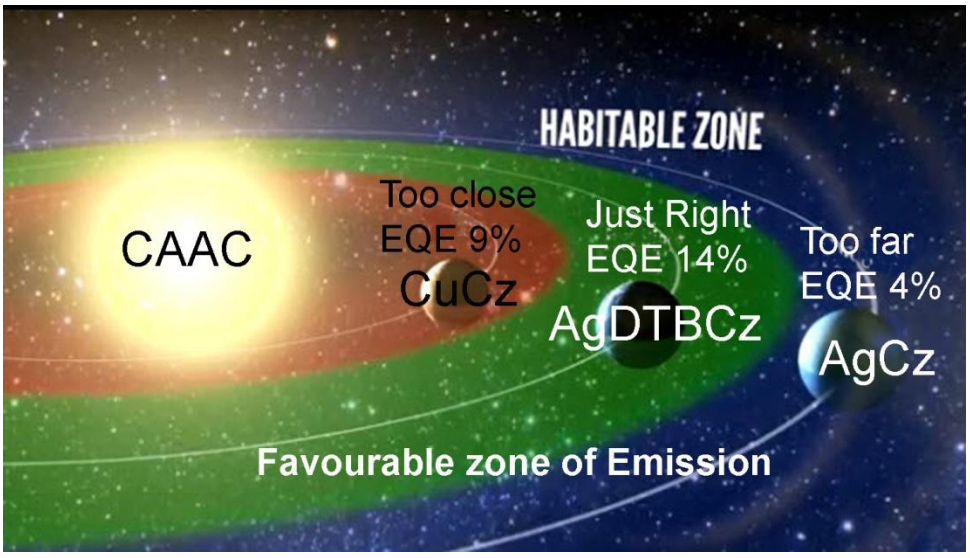

ABSTRACT:

Carbene metal amides (CMAs) are a new class of highly efficient light-emitting molecules based on a linear donor-metal-acceptor geometry. Here we report the synthesis, structure, photo- and electroluminescence of carbene silver carbazolato complexes, (^{Ad}L)Ag(Cz) [^{Ad}L = adamantyl-substituted cyclic (alkyl)(amino)carbene; Cz = carbazolate (**1**) and 3,6-^{t}Bu$_2$Cz (**2**)]. They display green emission with photoluminescence quantum yields of up to 74%. Efficient mixing of triplet and singlet excited states is observed, with sub-microsecond thermally activated radiative triplet lifetimes. These complexes provide prototype organic light-emitting diodes (OLEDs) based exclusively on silver emitters, with external quantum efficiencies of up to 14%.

Coinage metal complexes are noted for their ability to emit light by phosphorescence or thermally activated delayed fluorescence (TADF) mechanisms.[1] We have recently reported the synthesis and properties of photoemissive complexes of the type (CAAC)MX (M = Cu, Ag, Au; X = halide, aryloxide or amide; CAAC = cyclic alkyl(amino) carbene),[2-4] with amide complexes (X = NPh$_2$ or carbazolate) being particularly effective.[5] In these linear compounds the metal links CAAC carbene ligands with carbazolate (Cz) anions to give a rotationally flexible donor-metal-acceptor type structure. Using gold compounds (^{Ad}L)AuCz, organic light-emitting diodes (OLEDs) with near-100% internal quantum efficiencies at high brightness have been achieved.[5,6] However, there are currently no examples of practical electroluminescence (EL) devices based on mononuclear silver.[7] Indeed, OLED devices based on 2nd row metals in general are remarkably rare and characterized by low efficiency.[8] Here, we report silver complexes with sub-microsecond radiative triplet lifetimes and high performance in both solution and vacuum-deposited OLED devices.

Complexes **1** and **2** were readily obtained from (^{Ad}L)AgCl[3] and carbazole / NaO^{t}Bu as off-white (**1**) or yellow (**2**) solids (Figure 1). The compounds are stable for long periods of time both in air and in solution in non-protic organic solvents. Unlike many silver complexes, they are not sensitive to ambient light. Thermogravimetric analysis (TGA) gives decomposition temperatures (5% weight loss) of 264.8 (**1**) and 263.6 °C (**2**). The observation of the ^{13}C(carbene) NMR signal (δ_C 263) as two sharp ^{13}C–^{109}Ag and ^{13}C–^{107}Ag coupled doublets (J_{AgC} = 219 and 189 Hz, respectively) confirmed that the complexes do not undergo carbene ligand exchange.[9]

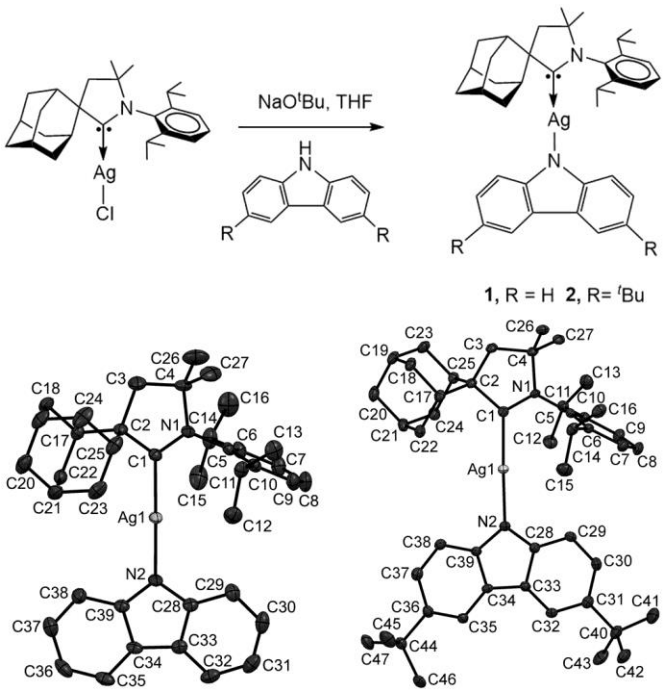

Figure 1. Synthesis and crystal structures of **1** and **2**·CH_2Cl_2. Ellipsoids are shown at 50% probability. Hydrogen atoms and CH_2Cl_2 molecule are omitted for clarity. For geometric parameters see Table 1.

Single crystal X-ray diffraction of **1** and **2** confirmed the mononuclear two-coordinate geometry and the absence of significant intermolecular contacts. The C1(CAAC)···N2(Cz) distance is of prime importance since it is directly related to the HOMO-LUMO overlap, which impacts on the radiative rate and exchange energy of (carbene)metal amides; this distance is slightly longer for **1** (4.152 Å) than for **2** (4.125 Å).

Table 1. Comparison of bond distances [Å] and angles [°] of the isostructural series (^{Ad}L)M(Cz) (M = Cu, Ag, Au).

(^{Ad}L)M(Cz)	M = Cu[a]	M = Ag, **1**	M = Ag, **2**	M = Au[a]
M1–C1	1.884(2)	2.085(2)	2.073(3)	1.991(3)
M1–N2	1.862(1)	2.067(1)	2.052(2)	2.026(2)
C1–N1	1.305(2)	1.294(2)	1.311(3)	1.299(4)
Angle C1–M1–N2	174.34(6)	178.55(7)	178.26(10)	178.78(11)
Torsion angle N1-C1-N2-C28	7.8	19.9(4)	16.2(3)	17.6

[a] From ref. [5].

Both **1** and **2** show a quasi-reversible one-electron metal-centered reduction process (THF solution, [^{n}Bu$_4$N]PF$_6$ as supporting electrolyte; SI, Figures S2, S3; Table S1). The estimated LUMO energies (**1**: -2.86 eV; **2**: -2.83 eV) compare well with those for the Au (-2.79 eV) and Cu analogues (-2.66 eV)[5] and are only marginally affected by the nature of the metal. The peak-to-peak separation ΔE_p is smaller for **2** (124 mV) than for **1** (185 mV), indicating higher stability of the reduced species of **2**, potentially making it a more robust emitter under electrical excitation. The HOMO levels based on the onset of the first oxidation potentials are at –5.51 and –5.29 eV for **1** and **2**, respectively. These values guide the identification of host materials for OLED fabrication.[10]

The electronic structure of **1** and **2** has been evaluated using density-functional theory (DFT) for the ground state and time-dependent DFT (TD-DFT)[11] calculations for the excited states using the MN15 functional by Truhlar[12] in combination with def2-TZVP basis set by Ahlrichs.[13-15] The calculated S_0 geometries are in good agreement with the crystal structures and the excited state energies suffer very little from the underestimation typical for TD-DFT.[16] Excitation involves a ligand-to-ligand charge transfer (LLCT) process from the carbazole to the carbene (SI, Figure S4, Tables S3, S4). Vertical $S_0 \rightarrow S_1$ excitation of **1** and **2** is dominated by the HOMO → LUMO transition (98%). The HOMO is mostly located on the carbazole with ca. 5% contribution from the silver atom, while the LUMO is centred on the $C_{carbene}$ p-orbital. The small d-orbital contributions are consistent with the insensitivity of the redox potentials of these compounds to the choice of metal. Distortion of the linear geometry was observed for the optimized S_1 and T_1 states: compared to S_0, the C1–Ag–N2 angle is 6–8° smaller, while the C–N (CAAC) bond is elongated by 0.07–0.09 Å, with simultaneous shortening of C1–Ag and elongation of N1–Ag bonds. Calculations suggest that the optimized S_1 structure is twisted by 41° for silver complexes (compared to 66° for copper and nearly 90° for gold analogues at the same level of theory). The relaxed S_1 energy is very weakly dependent on the dihedral angle, while T_1 has a stronger angular dependency (SI, Figure S15). The calculated exchange energy $\Delta E(S_1-T_1)$ for **1** and **2** at a 45° twist angle is 0.08 eV (645 cm^{-1}), while S_1 and T_1 states are approximately degenerate at full rotation.

The photophysical properties of the materials **1** and **2** were investigated using absorption and photoluminescence (PL) spectroscopy. CAAC and carbazole ligands show π–π* absorptions up to 360 nm which overlap with a broad ligand-to-ligand charge transfer LLCT

{π(carbazole)→π*(CAAC)} band at 388 and 400 nm for **1** and **2** in THF (Figure 2 and SI, Figures S5, S6, Table S2). Compared to **1,** the UV/vis profile of **2** in THF solution is red-shifted by 6 nm. Molar extinction coefficients for **1** and **2** at CT_{max} in THF are ~1 - 2 × 10^3 $M^{-1}cm^{-1}$, somewhat lower than those observed for Au and Cu analogues (~ 5 ×10^3 $M^{-1}cm^{-1}$)[5] and consistent with reduced HOMO-LUMO overlap owing to the larger C1-N2 distance. The position of the CT absorption edge blue-shifts by >50 nm (350 meV) with increasing solvent polarity, from benzene (dipole moment 0 D) to acetonitrile (3.92 D), and the relative extinction coefficient of the CT transition decreases.

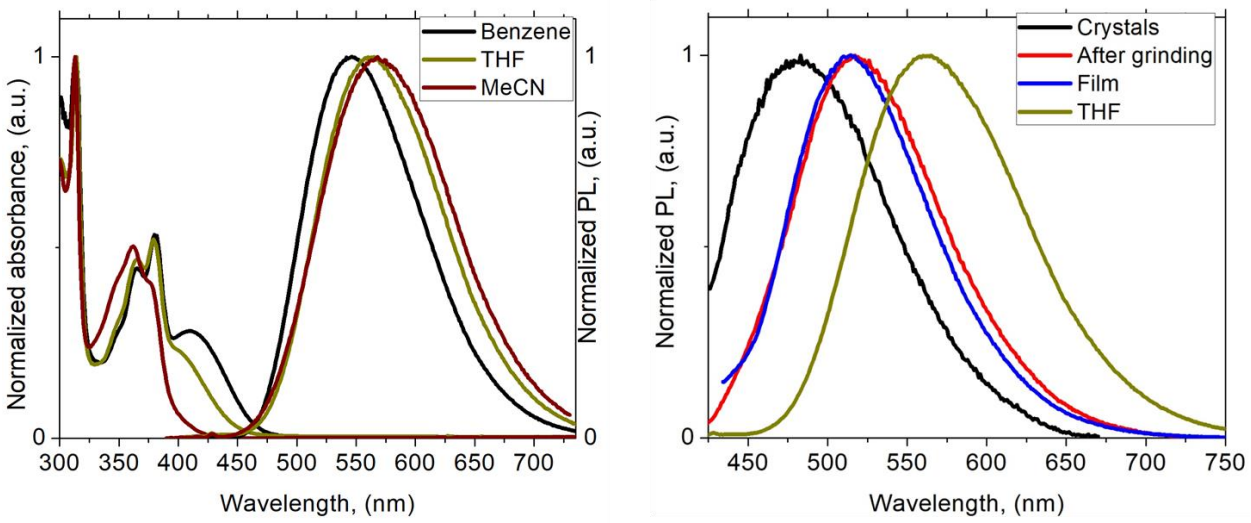

Figure 2. Left: UV-vis (normalized at 310 nm) and solution PL spectra (λ_{exc} = 380 nm) for **2**. Right: emission spectra (λ_{exc} = 380 nm) for **2** in various environments. Films were drop-cast from THF solutions and annealed at 80 °C for 5 min.

The steady-state PL properties, of **1** and **2** depend on the environment (Tables 2, SI Table S2). At 298 K both compounds exhibit broad and featureless green to yellow emissions, characteristic of CT–type excitations and consistent with calculations. Intact crystalline samples of **1** and **2** show low quantum yields (up to 17%) which are significantly improved by grinding (to 33%) or by drop-casting as thin films (to 45%). Processing samples in this way leads to a red shift by 30 nm compared to the as-crystallized sample (Figure 2; SI, Figures S9, S10), indicating that in the amorphous state lower-energy conformations are being accessed.

The emission peaks of **1** and **2** in a polymer matrix red-shift less than in neat solid films. The largest shift, by up to 85 nm (380 meV) compared to as-crystallized samples, occurs in solution. Solvent polarity induces a much smaller shift (by 20 nm, 85 meV), which suggests that geometric relaxation in the excited state is more important than stabilization by solvent dipoles. The contrast between excitation from the ground state versus relaxation from the excited state (350 meV vs. 85 meV shift with polarity) is in qualitative agreement with calculations indicating a reduced electric dipole moment in the excited state (11.9 D in the ground state vs. -4.9 D in S_1 geometry for **1**).[17,18] By contrast, organic TADF materials often show red-shifts of 100 nm or more with increasing polarity of solvent or polymer matrix.[17] PL quantum yields in degassed solutions drop from 74% (55%) to 19% (8%) for **1** (**2**) as solvent polarity increases. In deoxygenated solutions **1** and **2** exhibit monoexponential decays with lifetimes of ~200–500 ns (Table 2 and SI, Figure S13), implying radiative rate constants exceeding 10^6 s^{-1} at 300K. The emissions are strongly quenched by O_2, indicating the involvement of triplet states in the decay mechanism.

In solid films at 50 K, steady-state emission spectra of **1** and **2** blue-shift and develop additional structure (Figure 3a and SI, Figure S11). To understand this behavior, we turn to transient PL over a range of temperatures, measured using an electrically-gated ICCD camera. Figure 3b presents time-resolved PL decays for amorphous films of complex **2** (for decays of **1** see Figure S14). PL transients are characterized by non-exponential kinetics over three distinct time regimes – nanosecond (I), microsecond (II) and 100s of microseconds (III), with the latter significant only at low temperatures. The early-time decay (τ_I = 4 ns) exhibits no significant *T* dependence, but these lifetimes are likely limited by the ICCD instrument response (~ 3 ns). We assign (I) to prompt fluorescence, with an estimated energy in excess of 2.92 eV. Spectral deconvolution indicates that its emission spectrum is blue-shifted compared to that at later times (Figure 3a). Luminescence in regime (II) is unstructured and thermally activated, with an activation energy of 84 meV for **2** (108 meV for **1**, Figure S12) and lifetimes ranging from τ_{II} = 420 ns at 300K to 20 μs at 50 K (380 ns to 11 μs for **1**, Figure S14). This is consistent with a TADF-type emission process. We thus assign regime (II) to TADF from the reservoir of ^{3}CT states created following intersystem crossing from the photoexcited singlet.[19] We attribute the non-exponential decay to emission from an ensemble of such CT states in different local configurations within the solid film, consistent with a gradual red-shift in emission during the decay. This regime

accounts for > 90% of total emission at room temperature (note that the delayed fluorescence spectra at 50 and 298 K and the neat film spectrum are essentially superimposable, Figures 2 and 3a and SI, Figure S14). The time-averaged spectra closely match electroluminescence from OLED devices (*vide infra*). Peak emission energy in this regime blue-shifts at lower temperature (Figure 3c), with a greater shift for **1** than for **2**. We interpret this as a reduced capacity for geometrical relaxation of the excited state, restricting both ^{1}CT and ^{3}CT manifolds to higher energy. Below 150 K, a weak third component is distinguishable at long times (τ_{III} > 100 μs). The associated emission spectra are highly structured, and we assign (III) to phosphorescence from a local excitation on the carbazole ^{3}LE state. The energy of the ^{3}LE state was estimated from the emission spectrum at 50K obtained after a time delay of 250 μs and found to be 2.92 eV for **1** and 2.88 eV for **2**, and it is thus accessible to excitations at the high-energy edge of the CT manifold.

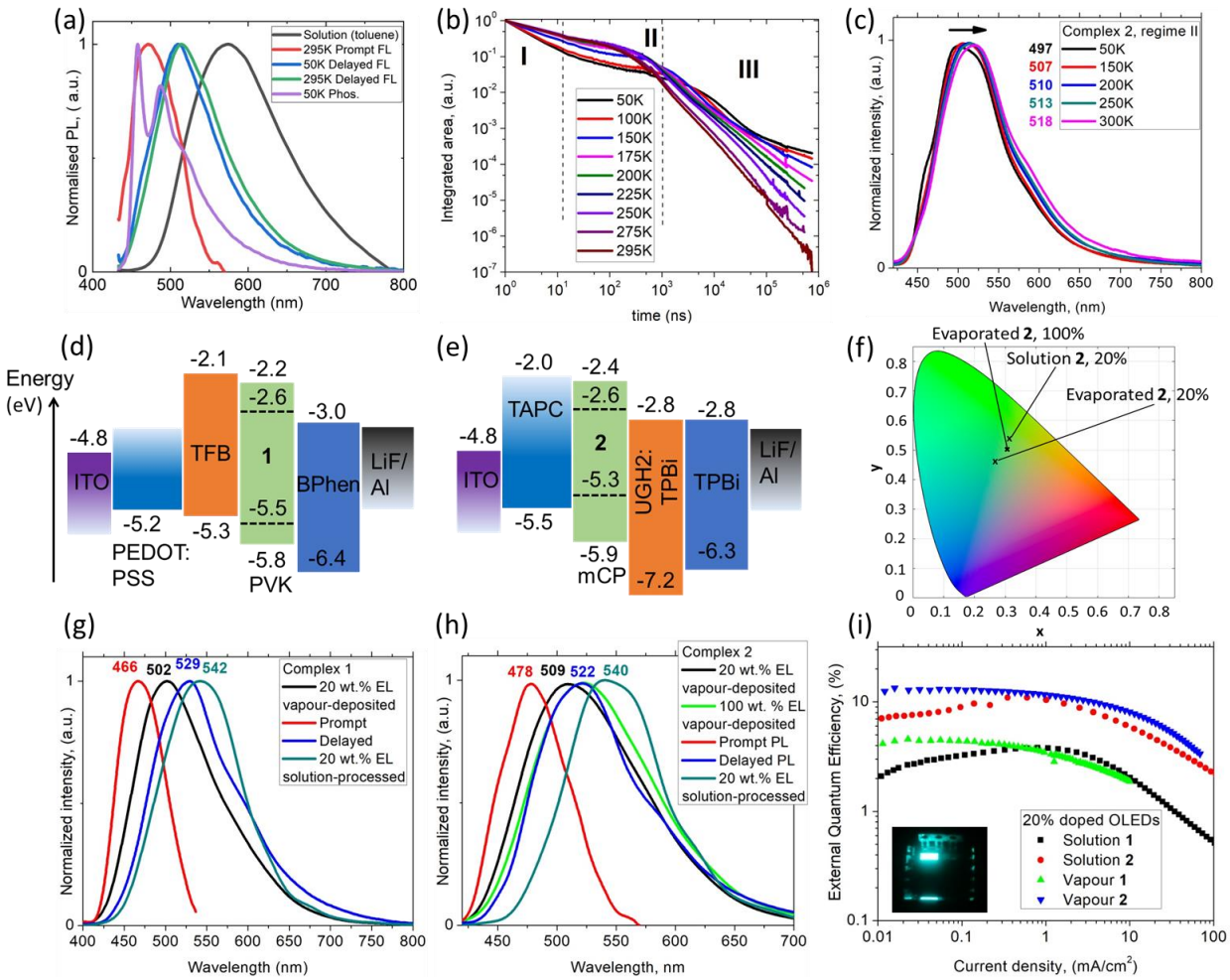

Figure 3. (a) Prompt (0-1 ns) fluorescence, delayed (100 ns) fluorescence and phosphorescence (250 µs) spectra for **2** in film at 295K and 50K, steady-state emission of **2** in toluene solution at 295K; (b) Time-resolved PL decay for films of **2** from 5 ns to 750 µs. (c) Temperature-dependent emission change for films of **2**. (d) Vapour-deposited and (e) solution-processed OLED devices architectures; (f) Commission International de l'Éclairage (CIE) colour co-ordinates of thermally evaporated and solution-processed OLEDs with complex **2**; (g) Electroluminescence (EL) and PL spectra for **1** and (h) for **2**; (i) External quantum efficiencies vs. current density of champion OLEDs based on **1** and **2**.

Table 2. Emission data of **1** and **2** in different environments.

	1			**2**		
	Film	toluene	PVK[a] matrix	film	toluene	PVK[a] matrix
λ_{em} (nm)	496	521	500	514	546	509
τ	380 ns (96%)	460 ns	358 ns	420 ns (96%)	305 ns	368 ns
Φ(%, 300K)	19[b]	74[c]	36[b]	45[b]	54.7[c]	44[b]
k_r (10^6 s^{-1})	0.5	1.6	1.0	1.1	1.8	1.2
k_{nr} (10^6 s^{-1})	2.1	0.6	1.8	1.3	1.5	1.5
E_a (meV)	108	–	–	84	–	–
$\Delta E(^1CT–^3LE)$		–0.08 eV[a]			–0.06 eV[a]	

[a] PVK = poly(9-vinylcarbazole); [b] PLQY under air; [c] PLQY under N_2.

We conclude that at ambient temperature the PL of both compounds **1** and **2** is dominated by a TADF-type process with low activation energy and rapid (sub-microsecond) triplet harvesting, rendering them promising candidates for OLED applications. To this end, both thermally-evaporated and solution-processed fabrication routes were explored.

Thermal vacuum deposition is the industry-preferred fabrication process, offering greater control and reproducibility at the expense of greater complexity and higher demands on thermal stability. The vapor-deposited OLED devices with architecture shown in Figure 3e give green emissions, with EL peaks dependent on dopant concentration. OLEDs with 20 wt-% and 50 wt-% dopant in 1,3-bis(9-carbazolyl)benzene (mCP) show EL peaks at λ_{em} = 502 (**1**, Figure 3g) and 509

nm (**2**, Figure 3h). Host-free devices show EL peak broadening and a red-shift to 521 nm, while the EL spectra closely match the microsecond-regime PL spectra. Figure S15 shows current density-voltage and luminance-voltage characteristics of evaporated devices with varying dopant concentrations. High external quantum efficiencies (EQEs) (for **2**: 12.9% at 100 cd/m^2 and 10% at 1000 cd/m^2) are achieved, with good roll-off characteristics. The maximum EQE is higher at low current-densities, indicating good charge balance, which is supported by the low turn-on voltage (Table 3).

Solution processing employed a multilayer OLED structure with all four organic layers being processed using orthogonal solvents, resulting in peak EQEs of 3.8% and 11.0% for **1** and **2,** respectively (Figures 3d and S15). Compared to vacuum-processed OLEDs the EL spectra are red-shifted,[20] and solution-processed devices made from **2** showed slightly increased roll off (11.0% at 200 cd/m^2 and 8% at 1000 cd/m^2), higher turn on voltage and reduced EQE at low current densities due to a slight imbalance in charge injection. This is to be expected given the difficulty in precisely controlling injection layer thickness in multilayer solution-processed architectures.

Table 3. Performance data of solution and evaporated OLEDs

Dopant [wt.%]/ Method	V_{ON} [V]	$\eta_{EQE,EL}$ [%] (Max.)	$\eta_{EQE,EL}$ [%] (100 cdm^{-2})	$\eta_{EQE,EL}$ [%] (1000 cdm^{-2})	CIE[a] (x,y)
1 [20] Evaporated	4.3	4.3	2.7	N/A	(0.26, 0.42)
1 [50] Evaporated	4.0	4.6	3.3	N/A	(0.25, 0.42)
2 [20] Evaporated	4.3	13.7	12.9	10.0	(0.28, 0.46)
2 [100] Evaporated	4.0	8.2	7.4	5.2	(0.31, 0.50)
1 [20] Solution	4.8	3.8	3.8	1.2	(0.35, 0.52)
2 [20] Solution	5.0	11.0	10.6	8.2	(0.36, 0.56)

[a] Commission Internationale de l'Éclairage (CIE) color co-ordinates

To conclude, (CAAC)silver amides are photo- and thermally stable TADF emitters which show the largest donor···acceptor separation in the coinage metal triad and give high radiative rates for triplet harvesting. Calculations indicate that the S_1 excited state geometry experiences

significant deviation from linearity, while the ligand-plane twist angle is the lowest in the isostructural coinage metal series. Efficient vapour- and solution-processed OLEDs have been fabricated with EQEs up to 12.9% at practical brightness, and a maximum luminance of 21,000 cd/m^2. The results show that lighter, cheaper and more abundant 2nd row elements may provide an as-yet little tapped resource for emitter materials.

Acknowledgements

This work was supported by the European Research Council, the Royal Society. M. B. is an ERC Advanced Investigator Award holder (grant no. 338944-GOCAT). D.C. acknowledges support from the Royal Society (grant nos. UF130278 and RG140472). The computations were made possible by use of the Finnish Grid Infrastructure resources (urn:nbn:fi:research-infras-2016072533). We thank S. Polonius and A. Reponen for assistance with initial data.

Supporting Information

For Supporting Information and crystallographic data in CIF or other electronic format see DOI: 10.1039/XXXXXX. CCDC number 1832143 for **1** and 1832142 for **2** contains the supplementary crystallographic data for this paper. These data can be obtained free of charge from the Cambridge Crystallographic Data Centre via www.ccdc.cam.ac.uk/data_request/cif.

References

[1] a) C. Bizzarri, F. Hundemer, J. Busch, S. Bräse, *Polyhedron*, **2018**, *140*, 51-66; b) H. Yersin, R. Czerwieniec, M. Z. Shafikov, A. F. Suleymanova, *Chem. Phys. Chem.*, **2017**, *18*, 3508-3535; c) Y. Zhang, S. R. Forrest, *Phys. Rev. Lett.*, **2012**, *108*, 267404; d) H. Yersin, *Highly Efficient OLEDs with Phosphorescent Materials*, Wiley-VCH, Weinheim, 2008; ISBN 978-3-527-40594-7; e) M. A. Baldo, D. F. O'Brien, Y. You, A. Shoustikov, S. Sibley, M. E. Thompson, S. R. Forrest, *Nature*, **1998**, *395*, 151-154.

[2] A. S. Romanov, D. Di, L. Yang, J. Fernandez-Cestau, C. R. Becker, C. E. James, B. Zhu, M. Linnolahti, D. Credgington, M. Bochmann, *Chem. Commun.* **2016**, *52*, 6379-6382 and **2018**, *54*, 3672.

[3] A. S. Romanov, M. Bochmann, *J. Organomet. Chem.* **2017**, *847*, 114-120.

[4] A. S. Romanov, C. R. Becker, C. E. James, D. Di, D. Credgington, M. Linnolahti, M. Bochmann, *Chem. Eur. J.*, **2017**, 23, 4625–4637. b) M. Gernert, U. Meller, M. Haehnel, J. Pflaum, A. Steffen, *Chem. Eur. J.* **2017**, *23*, 2206-2216; c) R. Hamze, R. Jazzar, M. Soleilhavoup, P. I. Djurovich, G. Bertrand, M. E. Thompson, *Chem. Commun.* **2017**, *53*, 9008-9011.

[5] D. Di, A. S. Romanov, L. Yang, J. M. Richter, J. P. H. Rivett, S. Jones, T. H. Thomas, M. A. Jalebi, R. H. Friend, M. Linnolahti, M. Bochmann, D. Credgington, *Science*, **2017**, 356, 159–163.

[6] P. J. Conaghan, S. M. Menke, A. S. Romanov, S. T. E. Jones, A. J. Pearson, E. W. Evans, M. Bochmann, N. C. Greenham, D. Credgington, *Adv. Mater.*, **2018**, *30*, 1802285.

[7] OLEDs based on Ag-Pt clusters have been reported: H.-X. Shu, J.-Y. Wang, Q.-C. Zhang, Z.-N. Chen, *Inorg. Chem.* **2017**, *56*, 9461−9473; b) Y.-P. Li, X.-X. Fan, Y. Wu, X.-C. Zeng, J.-Y. Wang, Q.-H. Wei, Z.-N. Chen, *J. Mater. Chem. C,* **2017**, *5*, 3072-3078.

[8] Ru and Pd based OLEDs have been reported, with EQEs <1%: (a) J. Yang, K. C. Gordon, Chem. Phys. Lett. 2003, 372, 577–582. (b) H. Xia, C. Zhang, X. Liu, S. Qiu, P. Lu, F. Shen, J. Zhang, Y. Ma, *J. Phys. Chem. B* **2004,** *108*, 3185-3190. (c) A. F. Henwood, M. Lesieur, A. K. Bansal, V. Lemaur, D. Beljonne, D. G. Thompson, D. Graham, A. M. Z. Slawin, I. D. W. Samuel, C. S. J. Cazin, E. Zysman-Colman, *Chem. Sci*. **2015**, *6*, 3248–3261

[9] H-L. Su, L. M. Perez, S-J. Lee, J. H. Reibenspies, H. S. Bazzi, D. E. Bergbreiter, *Organometallics*, **2012**, *31*, 4063-4071.

[10] C.M. Cardona, W. Li, A.E. Kaifer, D. Stockdale, G.C. Bazan, *Adv. Mater.*, **2011**, *23*, 2367-2371.

[11] F. Furche, D. Rappoport, Density functional methods for excited states: equilibrium structure and electronic spectra. In: *Computational Photochemistry*; M. Olivuccim, Ed.; Elsevier: Amsterdam, 2005; pp. 93–128.

[12] H.S. Yu, X. He, S.L. Li, D.G. Truhlar, *Chem. Sci*. **2016**, *7*, 5032–5051.

[13] F., Weigend, M. Häser, H. Patzelt, R. Ahlrichs, *Chem. Phys. Lett.* **1998**, *294*, 143–152.

[14] F. Weigend, R. Ahlrichs, *Phys. Chem. Chem. Phys.* **2005**, *7*, 3297–3305.

[15] D. Andrae, U. Haeussermann, M. Dolg, H. Stoll, H. Preuss, *Theor. Chim. Acta* **1990**, *77*, 123–141.

[16] A. Dreuw, M. Head-Gordon, *Chem. Rev.* **2005**, *105*, 4009–4037.

[17] J. Föller, C.M. Marian, *J. Phys. Chem. Lett.*, **2017**, *8 (22)*, 5643–5647.

[18] a) F. B. Dias, T. J. Penfold, A. P. Monkman, *Methods Appl. Fluoresc.* **2017**, *5*, 012001; b) M. K. Etherington, J. Gibson, H. F. Higginbotham, T. J. Penfold, A. P. Monkman, *Nat. Commun.* **2016**, *7*, 13680; c) K. Suzuki, S. Kubo, K. Shizu, T. Fukushima, A. Wakamiya, Y. Murata, C. Adachi, H. Kaji, *Angew.Chem. Int. Ed.* **2015**, *54*, 15231–15235.

[19] T. Hosokai, H. Matsuzaki, H. Nakanotani, K. Tokumaru, T. Tsutsui, A. Furube, K. Nasu, H. Nomura, M. Yahiro, C. Adachi, *Sci. Adv.*, **2017**, *3*, e1603282.

[20] Similar correlations were reported for vapour-deposited OLED devices with (^{Ad}L)Au(carbazolate), ref. [6].